Bull Eng Geol Environ
DOI 10.1007/s10064-017-1164-7

ORIGINAL PAPER

Liquefaction response of loose gassy marine sand sediments under cyclic loading

Yong Wang[1,2] · **Lingwei Kong**[1] · **Yanli Wang**[3] · **Mingyuan Wang**[4] · **Min Wang**[5]

Received: 15 January 2017 / Accepted: 19 September 2017

Abstract Gassy sediments have often been encountered in the marine seabed, and they have different features from common saturated and unsaturated soil. By developing and improving an effective methodology, triaxial gassy sand specimens with different initial gas content (saturation ≥85%) were prepared in the laboratory. Their state parameters can be controlled in real time. A series of undrained dynamic triaxial tests by a Global Digital System (GDS) dynamic testing apparatus were conducted to investigate the liquefaction characteristics of gassy sand sediments. The results show that the gassy sand can liquefy the same as the fully saturated sand, but gas existence monotonically increases the sand liquefaction resistance. The occluded gas bubbles have significant influences on sand liquefaction properties. The dynamic pore pressure of gassy sand shows obvious features of slower accumulation, greater amplitude fluctuation, and deeper groove shape in time history curves of pore water, resulting from the effects of gas compression/expansion, migration, and dissolution/exsolution. By introducing a parameter of saturation, a modified model was proposed to describe the evolution of dynamic pore pressure of gassy sands. It was found that the model parameter θ is linearly dependent on the initial gas content (or initial saturation degree S_r).

Keywords Marine sediments · Gassy sand · Gas content · Cyclic loading · Liquefaction

Introduction

Gas can be found in many soils, but most common in gas-charged sediments. Gas-charged sediments are known to be widely distributed throughout the world's marine, lacustrine, or interactive marine and terrestrial sedimentary environments (Fleischer et al. 2001). The origin of gas has been attributed to the upward migration of biogenic and/or petrogenic (thermogenic) gases from deeper parts of sedimentary layers (Lee and Chough 2003; Oung et al. 2006). In most occasions, the predominant gas is methane, and it presents in sediments in three ways: solution in the pore water, undissolved in the form of gas-filled voids, or as gas hydrates (Sills and Wheeler

✉ Yong Wang
wang831yong@126.com

Lingwei Kong
lwkong@whrsm.ac.cn

Yanli Wang
wyldhh@126.com

Mingyuan Wang
409976046@qq.com

Min Wang
sacewangmin@gmail.com

[1] State Key Laboratory of Geomechanics and Geotechnical Engineering, Institute of Rock and Soil Mechanics, Chinese Academy of Sciences, Wuhan, Hubei 430071, People's Republic of China

[2] State Key Laboratory for Geomechanics and Deep Underground Engineering, Xuzhou, Jiangsu 221116, People's Republic of China

[3] Key Laboratory of Geotechnical Mechanics and Engineering of the Ministry of Water Resources, Yangtze River Scientific Research Institute, Wuhan, Hubei 430010, People's Republic of China

[4] Power China Huadong Engineering Corporation, Hangzhou, Zhejiang 311122, People's Republic of China

[5] Rockfield Software Ltd, Swansea SA1 8AS, UK

Published online: 05 October 2017

1992). Because gas hydrate is usually formed in high pressure and low temperature environments, occurring in deeper regions (depths ≥300 m), the methane found in most marine sediments of the seafloor in shallow seas (depths <300 m) is water-soluble or in the form of free gas.

Direct observations in shallow marine gas-charged sediments revealed that the gas phase is discontinuous forming discrete, isolated bubbles, but a continuous water phase within voids (Sills et al. 1991; Christan et al. 1997; Anderson et al. 1998; Boudreau et al. 2005). Sparks (1963) and Nageswaran (1983) argued that the critical water saturation for the gas phase to be discontinuous is about 0.85. Fredlund and Rahardjo (1993) also believed that when the degree of water saturation is higher than 85%, the gas bubbles exist as isolated bubbles within the voids. This paper aims to investigate properties of the marine gas-charged sand sediments with initial saturation above 85%.

The marine gas-charged sediments are deemed a gassy soil, which is different from common saturated soil and general unsaturated soil. The features that make these sediments different from saturated soil are unique, but there is no single analytical expression of classifiable attributes for the soil to define the boundary between them and unsaturated soil. Sobkowicz and Morgenstern (1984) used the term "gassy soil" to denote soils that contain volumes of gas dissolved in the pore fluid either because of the high solubility of the gas or high fluid pressures. Through the observed behaviors, he gave a diagram to illustrate the differences in behavior between common unsaturated and gassy soils, as shown in Fig. 1. Gassy soil subjected to an undrained decrease in total stress has an equal decrease in pore pressure until a liquid-gas saturation pressure is reached. Then, gas exsolution begins at this point, and the pore pressure remains near the saturation pressure for a continual decrease in total stress, which results in that the effective stress decreases significantly with the changes of total stress. As the effective stress becomes very small, the soil compressibility increases, and the pore pressures begin to decrease. Hence, it can be seen that even though gassy soil is unsaturated, its mechanical behaviors are different from the general unsaturated soil.

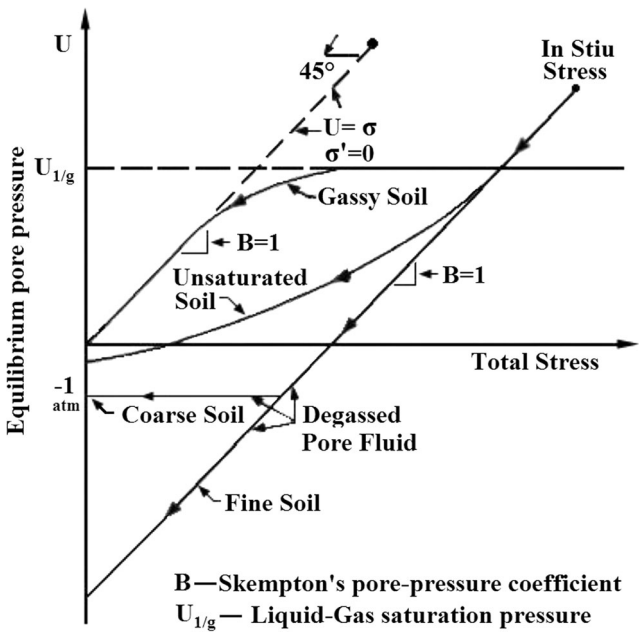

Fig. 1 Undrained equilibrium behavior of gassy soil and unsaturated soil under unloading

In recent years, marine gassy sediments have been reported to be an adverse geological factor, posing a safety risk for near shore infrastructure, ferry terminals, ports, pipelines, cables, etc. (Wheeler et al. 1991; Van Kessel and van Kesteren 2002; Tjelta et al. 2007, Mabrouk and Rowe 2011). An important reason for this is that the dissolved or confined gas in sediments has significant effects on soil behaviors due to the change of external environment, such as load or temperature (Sills and Wheeler 1992, Grozic et al. 1999, Rebata-Landa and Santamarina 2012, Wang et al. 2017). The accumulation of gas in shallow seafloor sediments greatly affects the stability of these deposits when subjected to mechanical impact (earthquakes, drilling), hydraulic impact (wave, tidal current), or climate impact (storms). Even a small amount of gas present in marine environments could have significant geotechnical implications. Several properties of gassy soils under the conditions of static load have been investigated effectively (e.g. Esrig and Kirby 1977; Sills and Wheeler 1992; Sills and Gonzalez 2001; Amaratunga and Grozic 2009; Puzrin et al. 2011; Sultan et al. 2012; Rebata-Landa and Santamarina 2012). However, so far very limited research has been reported on their dynamic response, such as the features of liquefaction.

Several investigations about the cyclic resistance of unsaturated sands with different saturation degrees have been achieved through some typical studies. Yoshimichi et al. (2002) deduced relations between the B-value and the velocity of P-waves and S-waves and used the B-value to discuss the cyclic resistance of partly saturated sand. Ishihara et al. (2004) conducted series of undrained triaxial tests on the clean sand with saturation degree changing from 0.1 to 0.95 under cyclic loading conditions and revealed that the cyclic strength tends to increase apparently with decreasing level of saturation for the loose sand. Yoshimichi et al. (2014) conducted multiple undrained cyclic triaxial tests on two unsaturated silty sands to investigate their cyclic resistance. However, these studies focused on liquefaction properties of common unsaturated sand rather than gassy sand. Moreover, their specimen preparation methods of unsaturated sand are significantly different from that of gassy soil.

Grozic et al. (2000) firstly studied the response of loose gassy sand under undrained cyclic loading and concluded that the soil containing gas bubbles still experiences cyclic liquefaction, but its cyclic liquefaction potential is reduced by the

addition of gas. Combing Henry's law for dissolution of gas in water, Ahmad et al. (2007) proposed a constitutive formulation for simulating the behavior of gassy sand under seismic loads. By introducing powdered sodium perborate monohydrate into Ottawa sand to generate oxygen gas bubbles for gassy specimen preparation, Eseller-Bayat (2009) experimentally studied the seismic response of gassy sand and prevention of liquefaction failure. Subsequently, an empirical model was further developed to predict the pore pressure ratio in the sand subjected to earthquake-induced shear strains (Eseller-Bayat et al. 2013). However, it is worth noting that the above studies are mainly focused on liquefaction resistances of gassy sand, the evolution of dynamic pore pressure during the liquefaction, and effects of gas on liquefaction mechanism were seldom investigated in particularly. Therefore, more research is needed on exploring behaviors of liquefaction response for marine gassy sediments.

In view of the complexity of gassy sample preparation for triaxial tests in the laboratory, firstly, the study introduces a feasible methodology for preparing traxial gassy sand specimens in the lab. Then, based on a series of undrained cyclic triaxial tests on the gassy specimens with different initial saturation degree, different liquefaction properties and dynamic pore pressure evolutions between marine gassy sand and fully saturated sand are investigated under cyclic loading.

Laboratory program

We obtained gassy sediment samples to explore their engineering properties in the lab. Gassy sediments usually in a metastable equilibrium state in nature, and are the products of balance in combination with soil particles, pore water, pressure gas, temperature, and sealing barriers. They are so vulnerable that it is difficult to obtain undisturbed soil samples in the field; even if an undisturbed sample could be obtained with special equipment, the cost is very high. In addition, gassy sediment samples obtained in the field are difficult to use for secondary operations in lab, because usually they are inhomogeneous and discrete, not meeting the needs of general traxial tests. Developing a preparation method to reconstitute gassy specimens is important for studying their mechanical properties in the lab. Furthermore, it is the first step for indoor experimental tests, especially for the marine sediments bearing dissolved and free gas.

Test apparatus

In Fig. 2, an advanced stress path triaxial system with an inner pressure chamber produced by Global Digital System (GDS) Ltd. is used to prepare gassy soil specimens. The GDS is equipped with a bender-extender elements system (BES) and an electronic volume change device (VCD) for the double-walled traxial pressure chamber. BES can generate shear waves (i.e. S-waves) and also compression waves (i.e. P-waves) to test the wave velocity of soil specimens (Lings and Greening 2001; Gu et al. 2013). The VCD is connected between the inner and outer chamber for accurate measurement of the specimen's volume change. The schematic diagram of double-walled traxial pressure chamber and VCD are shown in Fig. 3.

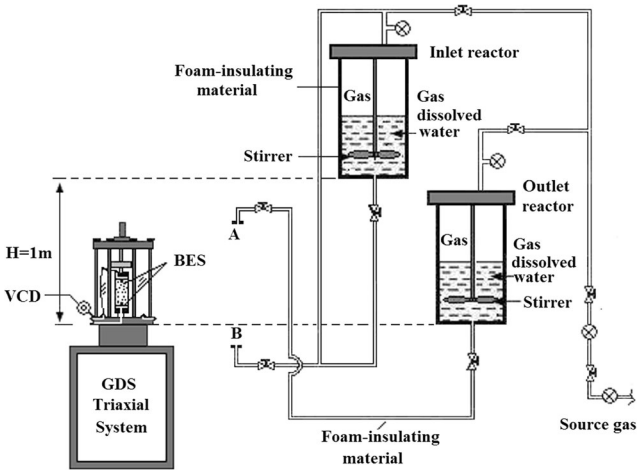

Fig. 2 Schematic of gassy specimen preparation system

In Fig. 2, right is a circulation system of constant temperature, which is similar to Grozic et al. (1999). It is a supporting apparatus for specimen preparation. The system consists of two high-pressure reactors (rated at 5 MPa) to prepare gas-dissolved water, partially filled with deaired distilled water. Meanwhile, the reactors and related connecting line are wrapped in foam-insulating materials to avoid influences on

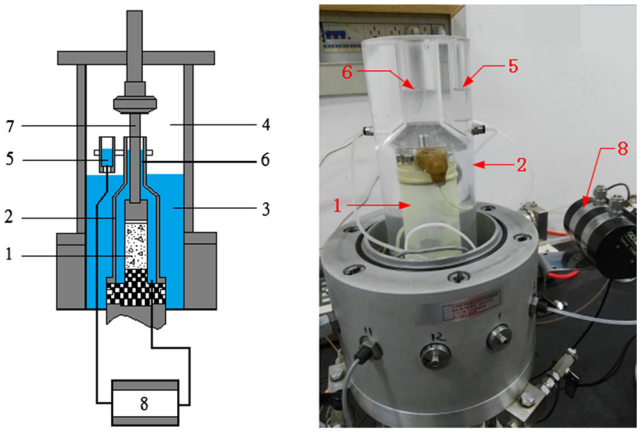

Fig. 3 The double-walled traxial pressure chamber and the volume change device (VCD). (a) schematic diagram for measurement of volume change; (b) image for installation of the inner chamber and VCD; 1—soil specimens, 2—inner chamber, 3—water for outer cell pressure, 4—gas for cell pressure, 5—water level in the reference tube, 6—water level in the inner chamber, 7—centre shaft for axial force, 8—VCD

gas solubility arising from the temperature variation. Although methane (CH_4) is the predominant gas found in marine seabed sediments, it has an inflammable and explosive nature, and it requires high pressure to dissolve in water (the solubility coefficient of CH_4 is approximately 0.034 L/L), which is a dangerous gas and usually forbidden in laboratories. Therefore, carbon dioxide (CO_2) was selected as the dissolved gas in reactors for preparing gassy specimens because of its safety nature in laboratory testing. As is well known, CO_2 leads to the stronger gas dissolution than methane gas (the solubility coefficient of CO_2 in water is 0.86 L/L at 20 °C). Grozic et al. (2005) concluded that the use of CO_2 leads to slightly conservative results from the viewpoint of engineering safety.

One of the high-pressure reactors is an inlet reactor, which is located 1.0 m above the cell of the GDS traxial apparatus and is connected to pipeline joint B; the other is an outlet reactor, which is parallel to the level of the triaxial cell and connected to pipeline joint A (in Fig. 2). Approximately 24 h prior to preparing specimens, the inlet and outlet reactors are charged with CO_2 gas to a higher pressure (usually over 800 kPa), which is the test dependent parameter. Each reactor has an electromagnetic stirrer installed to accelerate the dissolving balance of CO_2 gas into the deaired distilled water. After 24 h, the stirring stops and the work to prepare gas dissolved water is complete. Then, a fully saturated sand specimen with deaired distilled water is prepared by air-pluviation (Ladd 1977; Yamamuro and Wood 2004; Wood et al. 2008) in the cell of the GDS traxial system, and its pore water pressure is equal to the target pressure in reactors. Pipeline joint A is connected to the drainage port mounted on the pedestal, whilst joint B is connected to the drainage port connected to the cap at the top of soil specimens. The prepared gas-dissolved water in the inlet reactor is gravity-driven to flow through the saturated sand specimen from bottom to top into the outlet reactor because of the low hydraulic head difference, so that it can displace the deaired distilled water in pores of the soil. The circulation process takes about 2-3 h until the displaced water volume exceeded at least five times of the whole volume of sand specimens and there are no visible air bubbles in the circulation line. The flow rate is kept to minimize specimen disturbance. In the process of circulation, the pressure of CO_2 in the reactors controls the both pressure in the circulation system and the pore pressure of specimen.

Specimens preparation methodology

Remolded sand samples were collected from a typical exploration field of shallow gassy seabed in the Hangzhou Bay of China. The particle size is mainly distributed in the range of 0.25 mm ~0.075 mm. It is a type of silty sand with a nonuniformity coefficient of 19.7 and coefficient of curvature of 7.5. Before the testing, sand samples are dried and prepared for a traxial saturated specimen with the target initial dry density (1.280 g/cm^3) in the cell by the air-pluviation method. To achieve the full saturation, backpressure is ramped up to 800 kPa for most tests, whilst the cell pressure increases at the same time, maintaining a constant effective stress of 20 kPa. During the pressing, when the sand specimen is fully saturated, compressive wave velocities of over 1600 m/s are observed through the test of BES. By increasing cell pressure while maintaining the constant backpressure, the sand specimen is isotropic consolidated. The specimen's axial deformation is recorded using a linear voltage displacement transducer (LVDT), whilst volume changes are monitored by VCD. The consolidation process continues until the target mean effective stress (e.g. 50 kPa) is reached over 1 h. Then, specimens used for the gassy soil test go through a circulation stage before proceeding further according to the method in the previous section. After the prepared gas-dissolved water in the high-pressure reactors displaces the pore water of saturated specimen, the circulation system is disconnected and the specimen maintains an undrained condition for 0.5 h to ensure that the pressure stabilizes. At this point, the back valve is closed and the specimen is ready for isotropic undrained unloading. The cell pressure is reduced in a stepwise manner while the pore pressures and specimen volume change are recorded. For each step, the cell pressure is ramped (at 5 kPa/min) to unload 50 kPa. Then, keeping the pressure level, the pore pressure response of the specimen is carefully recorded and observed. This process usually lasts at least for 2 h. Meanwhile, the specimen height and volume variation are recorded at the same time. Meanwhile, the BES continuously produces P-waves to pass through the specimen, and the average wave velocities and wave forms are recorded.

In Fig. 4, at the beginning of unloading, the cell pressure and pore water pressure unloads simultaneously. The reduction of pore water pressure is the same as the cell pressure. For

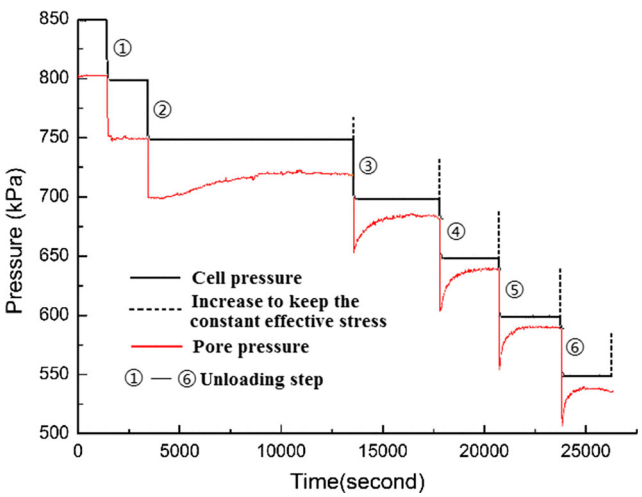

Fig. 4 Pore pressure response of gassy specimen during the isotropic unloading

instance, when the cell pressure unloads from 850 kPa to 800 kPa (step ①), the pore water pressure unloads from the initial pressure of 800 kPa to 750 kPa and the pressure stays level in the subsequent time. However, in the second unloading step, when the cell pressure unloads from 800 kPa to 750 kPa (step ②), the pore water pressure initially decreases from 750 kPa to 700 kPa, then it recovers to 719 kPa. Because of the undrained situation, gas exsolution results in recovered pore pressure. In this way, specimens with different initial gas content can be obtained through different numbers of unloading steps. Accordingly, the height and volume change of specimens are recorded during the unloading to calculate the state parameters for the specimens in each step, which will be illustrated in detail in the following section. When the last unloading step is over and the pore pressure is stable, the backpressure valve is opened and the backpressure is controlled at the same level as the current pore pressure, whilst the cell pressure is increased to recover to the mean effective stress (50 kPa). Then, the backpressure valve is closed and the undrained condition is maintained for a few minutes to allow the pressure to stabilize. Subsequently, BES is used to produce S-waves to test the shear wave velocity of the specimen under a constant effective stress of 50 kPa. If the test result does not differ much from that of the specimen at the fully saturated status, it can roughly demonstrate that the process of the gassy sample preparation is successful. Similarly, the gassy sand specimens with different initial saturation are prepared for the following triaxial liquefaction tests.

The speed of sound is very sensitive to gas bubbles, and even a small fraction of gas bubbles leads to a significant velocity decay (Kokusho 2000; Yong 2002). Therefore, the change of P-wave velocity excited by the BES can be an important signal for gas exsolution. In Fig. 5, it is the measured P-wave velocity of a specimen during the unloading. When the cell pressure changes from 800 kPa to 550 kPa, the velocity of the P-wave decreases from 1732 m/s to 792 m/s. Especially, when the cell pressure unloads from 750 kPa to 700 kPa, the measured P-wave velocity shows a significant decrease. This phenomenon demonstrates that there is a certain quantity of gas exsolution in the specimen. The measured S-wave velocity of a specimen during the unloading is shown in Fig. 6. It can be seen that the velocity of the S-wave is almost the same as the initial, which implies that there is almost no striking disturbance of soil skeleton. The P-wave is used to monitor the point of gas exsolution, and the S-wave is used to monitor the disturbance and help select a suitable reduction of the cell pressure in each unloading step. It is the reason why the BES should be equipped in GDS traxial system for the gassy specimen preparation.

It is worth noting that the point of gas exsolution is called the liquid/gas saturation pressure. It is true that the liquid/gas saturation pressure is not constant, and it is irrelevant to the mean effective stress and the initial density, only depending on the pressure that the gas is originally dissolved in water (Amaratunga and Grozic 2009). In fact, according to test experiences, the point of gas exsolution should be equal to the initial liquid/gas saturation pressure in the reactors (e.g.800 kPa). However, because the prepared gas-dissolved water in high-pressure reactors displaces the pore water of the saturated specimen at the mentioned circulation stage, the initial equilibrium point of liquid/gas saturation pressure in the reactors is broken by the attenuation of the deaired distilled water and then restored to a new balance again. This is why the point of gas exsolution is slightly lower than the initial backpressure (800 kPa). Nevertheless, it does not affect the normal experiment.

In order to slow and minimize the trend that high solubility of CO_2 in the specimen diffused into the confining fluid in the traxial cell, two latex membranes (0.3 mm thick inner membrane and 0.1 mm thick outer member) are used in all tests.

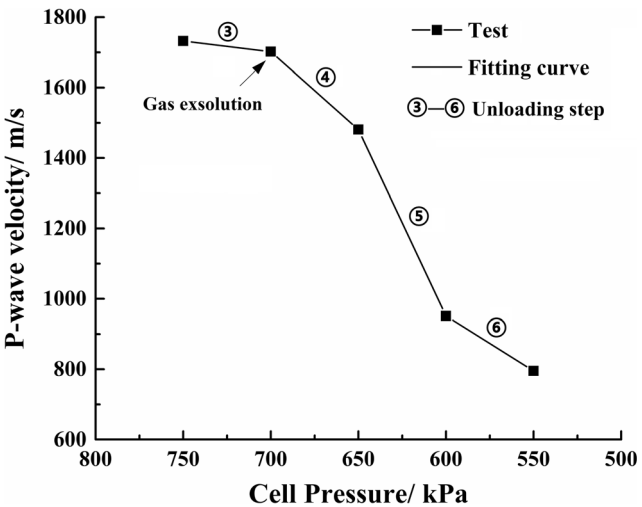

Fig. 5 P-wave velocity of the specimen during the unloading

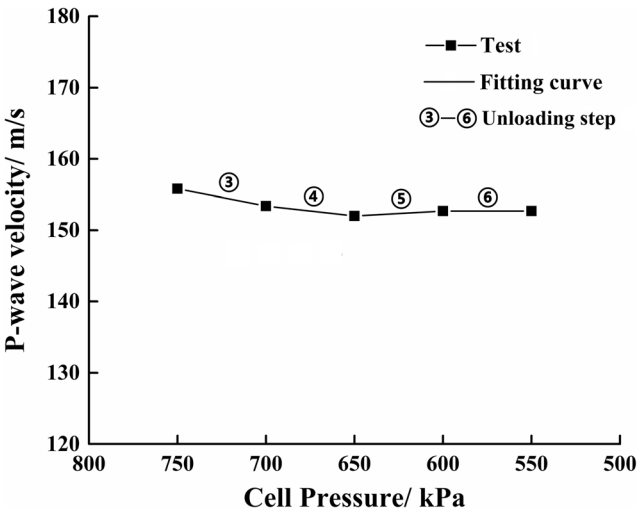

Fig. 6 S-wave velocity of the specimen during the unloading

Because the duration of the liquefaction test is not long, the problem of gas diffusion is not significant.

State parameters of specimens

As mentioned previously, the volume change of soils during specimen preparation has been recorded so that the state parameters, such as saturation, void ratio, and porosity, of specimens at different times can be calculated. The initial saturation degree of typical marine gassy sand sediments is usually in the range of high saturation (between 85% and 100%). At present, there is no effective experimental technique that can detect the small saturation change in this range directly, including the time domain reflectometry (TDR), because the accuracy of these methods cannot meet requirements. Therefore, an indirect method to calculate saturation is adopted in this paper.

As is known, the most distinctive property of marine gassy soil is its volume expansion arising from gas exsolution under unloading in the undrained situation. Therefore, the volume change is important evidence and a measurable index to obtain the state parameters of gassy specimens. During the undrained unloading, after reduction of cell pressure at each step, there is an associated change in the pore pressure. Because the influence of compressibility of the free gas, the immediate response is a small change for the pore pressure or effective stress. However, with further decrease of the cell pressure, gas exsolution significantly affected the pore pressure response as shown in Fig. 4. The true equilibrium behavior can be observed after all gas exsolution has been completed. Volume expansion is expected due to gas exsolution and expansion, when the stress level is lowered. This caused changes in the saturation degree and void ratio of specimens. Therefore, if the volume change of specimens is obtained, the state parameters of specimens can be updated in analysis before decreasing the cell pressure at the next step.

The pore fluid of a gassy soil consists of miscible fluids: pore water, dissolved gas, and free gas. Fredlund and Rahardjo (1993) demonstrated that Boyle's law for free gas and Henry's law for dissolved gas can be combined by applying Boyle's law to the total volume of both free and dissolved gas in the system. If ignoring the volume compressibility of water under the condition of normal temperature, the total volume of water is constant and the volume of dissolved gas in water can be assumed as a constant irrespective of the pressure at which it is dissolved. Hence, the dissolved gas volume before and after unloading is the same and equal to hV^w, where V^w is the volume of water, and h is the Henry's volumetric coefficient of solubility. Henry's constant varies for different gas/liquid combinations; for air/water h is 0.02, for CO_2/water h is 0.86, and for CH_4/water h is 0.034 (Rad et al. 1994). Then applying Boyle's law to the total volumes of gas before and after unloading,

$$P_1^g\left(V_1^{gf}+hV^w\right)=P_0^g\left(V_0^{gf}+hV^w\right) \tag{1}$$

where P^g is the absolute gas pressure, V^{gf} is the volume of free gas, and subscripts. "0", "1" refers to the initial and final conditions of current step respectively. The volume change of free gas after unloading ΔV^{gf} is described as

$$\Delta V^{gf}=V_1^{gf}-V_0^{gf} \tag{2}$$

By substituting Eq. (1) into Eq. (2),

$$\Delta V^{gf}=-\frac{\Delta P}{P_g^1}\left(V_0^{gf}+hV^w\right) \tag{3}$$

where $\Delta P=P_1^g-P_0^g$. Fredlund and Rahardjo (1993) believed that when gas bubbles exist as occluded bubbles in the voids, surface tension forces can be ignored. Then the water and gas bubble mixture can be deemed as a homogeneous medium, and the pore gas pressure and the pore fluid pressure can be assumed as equal. Assuming that the volume of soil particles is incompressible, the total volume change of specimen ΔV^t is equivalent to the volume change of pore gas ΔV^{gf}. Thus, through Eq. (3),

$$\Delta V^t=-\frac{\Delta P}{P_g^1}\left(V_0^{gf}+hV^w\right) \tag{4}$$

$$\frac{\Delta V^t}{V_0^t}=-\frac{\Delta P}{P_g^1}\left(\frac{V_0^v}{V_0^t}\right)\left(\frac{V_0^{gf}+hV^w}{V_0^v}\right) \tag{5}$$

where V_0^v is the initial pore volume of a specimen. Since $\frac{V^w}{V_0^v}=S_0$, $\frac{V_0^{gf}}{V_0^v}=1-S_0$, $\frac{V_0^v}{V_0^t}=n_0$, and the change of absolute pressure ΔP is equal to the change of gauge pressure Δu, thus

$$\frac{\Delta V^t}{V_0^t}=\frac{\Delta u(1-S+hS)n_0}{u_0-\Delta u} \tag{6}$$

where u_0 is the pore fluid pressure before unloading, and n_0 is the porosity of the specimen before the corresponding stress reduction. As mentioned previously, after unloading at each step, saturation, void ratio, and porosity values have to be updated.

The change in degree of water saturation can be calculated as

$$dS=\frac{V^v dV^w-V^w dV^v}{(V^v)^2} \tag{7}$$

Since it is assumed that water is incompressible in comparison to gas, the volume change of water $dV^w\approx 0$. Then,

$$dS=-\frac{V^w dV^v}{(V^v)^2}=-\frac{V^w}{V^v}\frac{dV^v}{V^t}\frac{V^t}{V^v}=-\frac{S}{n}\left(\frac{dV^v}{V^t}\right) \tag{8}$$

Substituting Eq. (6) for $\frac{dV^v}{V^t}$, the degree of water saturation after unloading can be written as

$$S_1 = S_0 - \frac{S_0}{n_0}\frac{dV^v}{V_0^t} \tag{9}$$

Subscripts "0", "1" denotes the initial and final conditions corresponding to each unloading step, respectively. Since the total volume change of specimen is equal to the volume change of pore, $dV^v \approx dV^t$, thus Eq. (9) can be rewritten as,

$$S_1 = S_0 - \frac{S_0}{n_0}\frac{dV^t}{V_0^t} \tag{10}$$

where both dV^t and V_0^t can be measured by tests. Similarly, the new void ratio and the porosity values can described as

$$e_1 = e_0 + (1 + e_0)\frac{dV^t}{V_0^t} \tag{11}$$

$$n_1 = n_0 + \frac{dV^t}{V_0^t} \tag{12}$$

With this method, the relevant parameters of gassy specimens prepared for liquefaction tests are calculated and shown in Table 1. The initial dry density of all specimens is 1.277 g/cm^3 (relative density D_r = 0.3) and the initial porosity n_0 is 52.3%. All of specimens are in the loose state. As the solubility of CO_2 significantly affect by the temperature, during the gassy specimen preparation, the indoor temperature and water temperature are controlled at 20 °C. Through the different numbers of unloading steps, sand specimens with four types of initial saturation are prepared in the lab as shown in Fig. 7 and are 100%, 97.6%, 94.1%, and 92.3%, respectively.

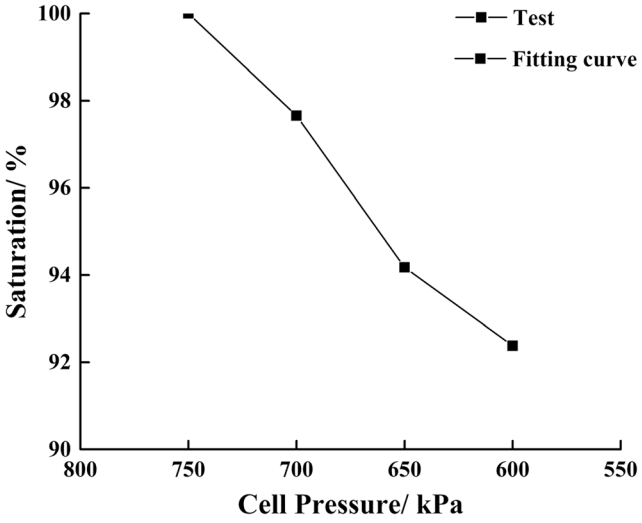

Fig. 7 Different initial saturations for the specimen preparation

Liquefaction tests and results

Test procedure

As shown in Fig. 2, the GDS triaxial apparatus is the Advanced Dynamic Triaxial Testing System (DYNNTTS), which is not only capable of achieving advanced stress path control tests, but also complex dynamical tests. The advanced stress path module of the system is used to prepare gassy specimens, whilst the dynamic module is used to conduct liquefaction tests. The dynamic system combined a triaxial cell with a dynamic actuator for applying load, deformation, and stresses up to 10 Hz. The cell itself is screw-driven from an integral base unit housing the motor drive. Axial force or deformation is applied through the base of cell, which can be applied with sinusoidal, half sinusoidal, triangular, and square waves, and user-defined waveforms. It can achieve high precision volume change measurement (VCD) and electromagnetic control. A high-speed direct current servo motor is used to apply the dynamic load (Axial load), and the size of load or deformation is output by a computer control according to feedbacks of the electronic load sensor and displacement sensor. The system can be combined with a dynamic cell pressure actuator such that cell pressures can also be applied dynamically up to fundamental frequency of the machine (Radial load). The apparatus consists of the following components: brake unit, triaxial cell pressure chamber and balancer, cell pressure controller, backpressure controller, signal controller, high-speed data acquisition, and control card (HSDAC card).

Table 1 Parameters for the gassy specimen preparation

Initial void ratio e_0	Henry's constant h	Unloading step	Unloading cell pressure (kPa)	Stabilizing pore pressure (kPa)	Total volume change $\triangle V^v$ (mm^3)	Type of saturation Sr (%)	Gas content n_g' (%)	P-wave velocity Vp (m/s)	S-wave velocity Vs (m/s)
1.098	0.86	②	750	719	0	100	0	1732	156
		③	700	684	1000	97.6	2.4	1702	153
		④	650	639	1640	94.1	5.9	1481	152
		⑤	600	590	6520	92.3	7.7	951	153
		⑥	550	537	13,040	90.8	9.2	792	153

After the gassy specimens are prepared with this method reached the target saturation, they are under isotropic consolidation at a uniform effective confining pressure (50 kPa). Once the volume of the specimen stays unchanged for 5 min, consolidation equilibrium is achieved, then the cyclic load is applied. The vibration waveform is the sinusoidal cycles with frequency of 0.2 Hz. Four different initial saturations (or gas contents) were selected for the sand specimens to carry out liquefaction tests. Each type of saturation was prepared for four specimens, and they were applied four different amplitude dynamic stresses under the same effective confining pressure, respectively, until the soil pore pressure reached the effective confining pressure. This means soil liquefaction is achieved.

Test results

Comparison of the deviator stress responses

The typical dynamic triaxial test results, including time histories of deviator stress, axial stress, and dynamic pore pressure of a saturated and a gassy sand are shown in Figs. 8 and 9, respectively. For the fully saturated sand, the applied deviator stress of the saturated specimen is 20 kPa, and the number of cycles to failure is 11. For the gassy sand (S_r = 92.3%), the applied deviator stress of gassy specimen is 35 kPa, and the number of cycles to failure is 33. Under cyclic loading, pore pressure developed in both saturated specimens and gassy specimens, which resulted in the reduction of effective confining pressure.

In Fig. 8(a), the deviator stress amplitude of the saturated specimen basically remained unchanged during the early stress cycles, then a sharp decrease in the deviator stress amplitude was observed just before the initial liquefaction occurred for one or two stress cycles. In comparison, in Fig. 9(a), the deviator stress amplitude of the gassy specimen shows the same response as that of the saturated specimen at the beginning, but there is no sharp reduction. It decreases gradually until the initial liquefaction occurs.

Comparison of the axial strain responses

The saturated specimen and the gassy specimen have different axial strain responses. In Fig. 8(b), the axial strain of the saturated accumulates slowly with increasing numbers of loading cycles before the initial liquefaction, and the amplitudes of tensile and compression strain are symmetrical. When the initial liquefaction occurs, the accumulative axial strain increases sharply in a compressive direction. Then only the total axial strain develops, but not the cyclic strain amplitude in each loading cycle. Comparatively, in Fig. 9(b), due to effects of gas expansion and exsolution arising from unloading, the amplitudes of tensile and compressive strain of the gassy

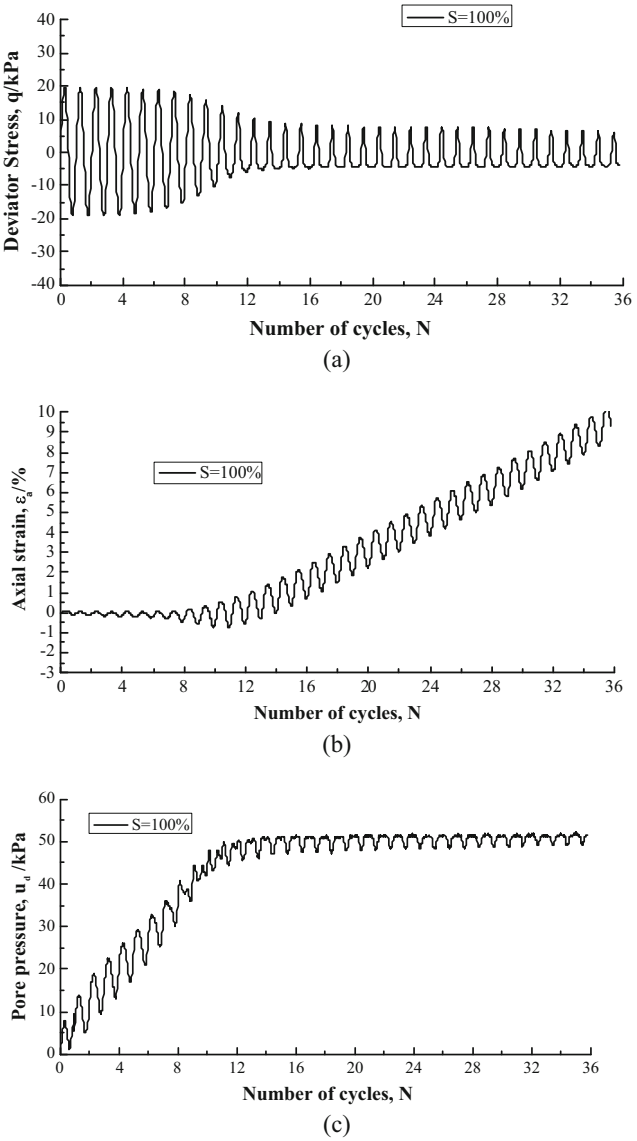

Fig. 8 Typical time history curves of a fully saturated specimen

specimen are unsymmetrical at the initial stage of cyclic loading, and the axial strain firstly accumulates in the tensile direction quickly. Meanwhile, the cyclic strain amplitude in each loading cycle increases slightly. When the initial liquefaction occurs, the cyclic strain amplitude in each loading cycle increases continuously. Once the stability of gas exsolution is achieved, the tensile strain amplitude begins to decrease. Whilst the compressive strain amplitude increases until the accumulative axial strain begins to decrease. Compared with the saturated specimen, amplitude of axial strain of the gassy specimen fluctuates greatly in process of a stress cycle.

Comparison of the dynamic pore pressure responses

In Figs. 8(c) and 9(c), the dynamic average pore pressures of saturated specimen and gassy specimen accumulate

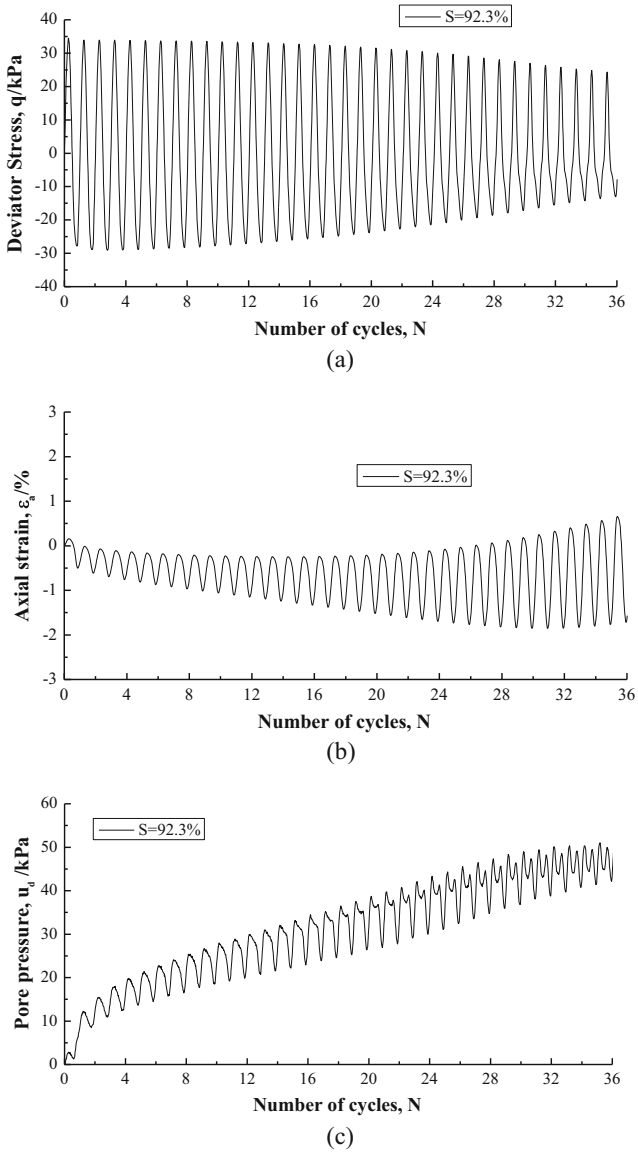

Fig. 9 Typical time history curves of a gassy specimen

monotonically with the increasing numbers of loading cycles, whilst the periodic fluctuation presents with the varying of dynamic load. For the saturated specimen, dynamic pore pressure develops steadily until liquefaction occurs at the 11th stress cycle. A groove shape near the wave crest in the time history curve of dynamic pore pressure begins to appear at the 9th stress cycle. At that time, the accumulative pore pressure approaches above 80% of that level at the initial liquefaction (about 40 kPa). In comparison, for the gassy specimen, the dynamic pore pressure develops much more rapidly at the first and second stress cycles, then it develops steadily, but the amplitude increases greatly in a stress cycle. The groove shape near the wave crest begins to appear at the 18th stress cycle, when the accumulative pore pressure is closed to 60% of that level at the initial liquefaction (about 30 kPa). Moreover, the depth of grooves is larger than that of the saturated specimen. As a whole, even though the dynamic pore pressure of gassy specimen accumulates slowly, its amplitude fluctuates largely in a stress cycle in accord with the development of axial strain. This is attributed to the existence of gas compression/expansion, migration, exsolution/dissolution during cyclic loading, which leads to more complex volume change of the sand skeleton.

Comparison of the stress-strain hysteresis loops

In Fig. 10(a) and (b), they are the typical stress-strain hysteresis loops of a fully saturated specimen. Figure 10(a) shows the 1st to 3rd stress cycles, and Fig. 10(b) shows the 9th to 11th stress cycles. The stress-strain hysteresis loop of the saturated specimen is irregular oval, and little change occurs between the adjacent hysteresis loops. The specimen can be considered still in the stage of visco-elasticity from the 1st to 3rd stress cycles. With the increase of stress cycles, stress-strain hysteresis loops are obviously changed, and differences between adjacent hysteresis loops gradually get larger from 9th to 11th stress cycles. The stress-strain hysteresis loops changes from sloping to horizontal direction with a recession in stiffness of the specimen. Then the initial liquefaction occurs. However, the gassy sand specimen shows a significantly different behavior from the saturated specimen. Figure 11(a) and (b) shows the typical stress-strain hysteresis loops from the 1st to 3rd and the 9th to 11th for the gassy specimen,

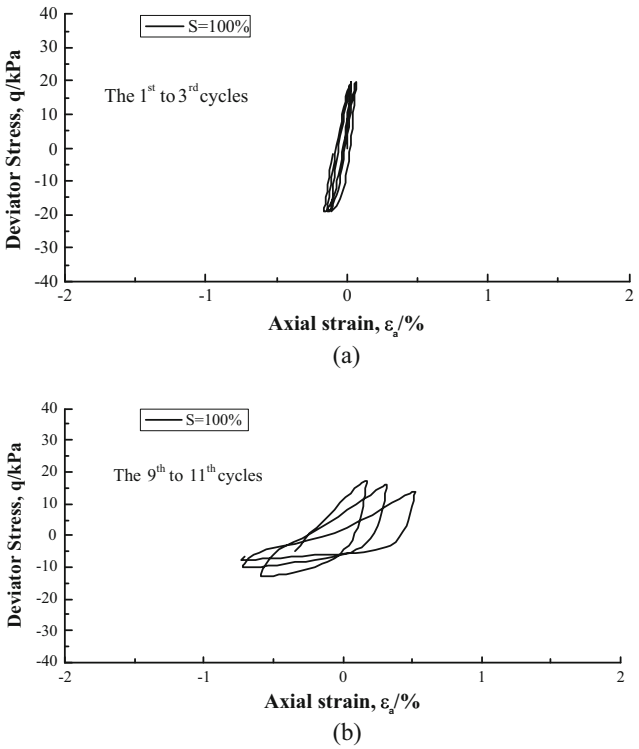

Fig. 10 Typical stress-strain hysteresis loops of a fully saturated specimen

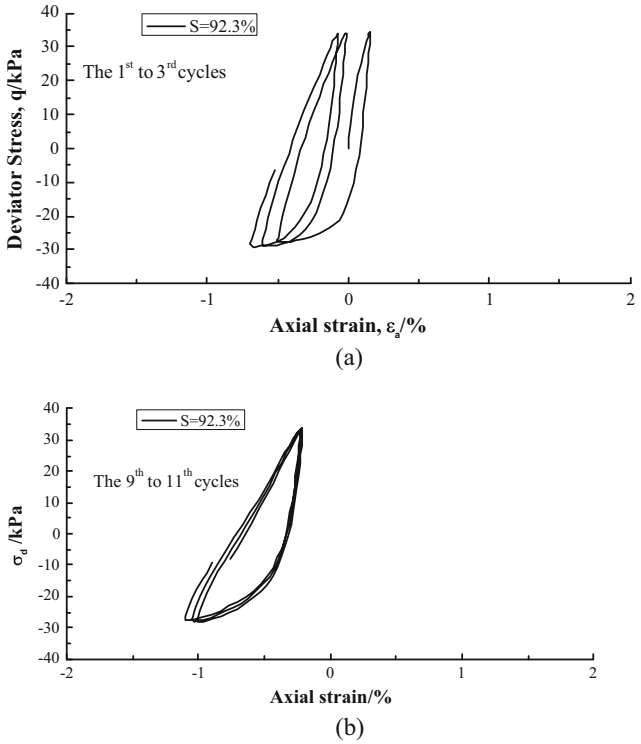

Fig. 11 Typical stress-strain hysteresis loops of a gassy specimen

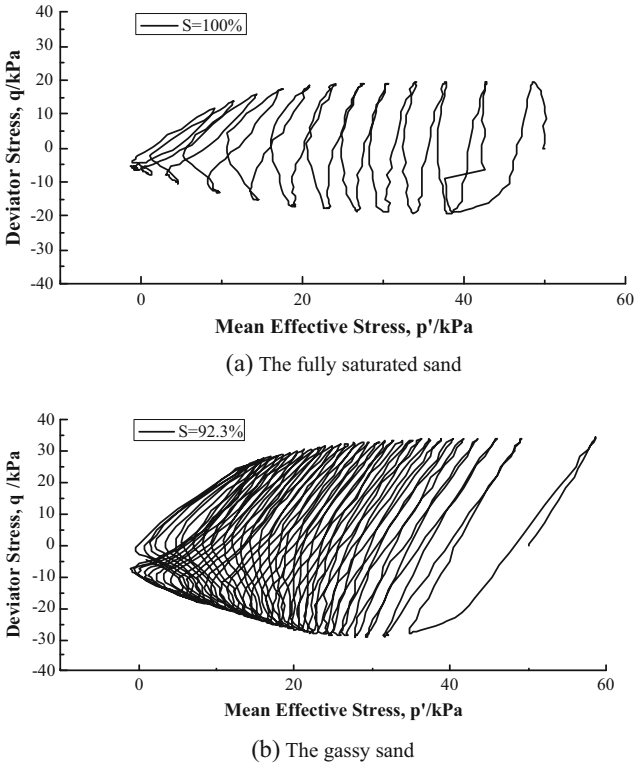

Fig. 12 Typical effective stress paths of a fully saturated and a gassy specimen

respectively. It can be seen in Fig. 11(a) that due to the higher resistance of gas bubbles freely passing through the sand voids (migration), under the action of dynamic stress, more energy is consumed to overcome the resistance. The stress-strain hysteresis loop of the gassy specimen is not oval and the larger change occurs between the adjacent of hysteresis loops from 1st to 3rd stress cycles. The tensile strain amplitude increases, whilst the compressive strain amplitude decreases. It illustrates that the structure of gassy specimen is not stable in the initial cyclic loading. With the increase of stress cycles, the tensile strain amplitude continuously increases, whilst the compressive strain amplitude decreases. However, differences between adjacent hysteresis loops gradually reduce from 9th to 11th stress cycles (in Fig. 11(b)). The stress-strain hysteresis loops between the 1st to 3rd and 9th to 11th stress cycles are both sloping, which implies that the gassy sand has higher residual cyclic loading resistance.

Comparison of the effective stress path

Figure 12(a) and (b) shows the difference in effective stress path between a saturated and a gassy specimen. In Fig. 12, the accumulation of dynamic pore pressure causes the mean effective principal stress of samples to decrease, and the effective stress paths of the fully saturated specimen and gassy specimen both move toward the original point. The stress path of the fully saturated specimen is subjected to a deviatoric stress of 20 kPa. Dynamic pore pressure begins building immediately and the mean normal effective stress decreases until the liquefaction occurs at the 11th cycle. Comparatively, the gassy specimen is subjected to a deviator stress of 35 kPa, and the number of cycles to failure is 33. Reaching the initial liquefaction needs much more stress cycles, which shows that the gassy sand has a greater liquefaction resistance than the fully saturated sand.

Comparison of the liquefaction mechanism

Through this study, it can be found that there are some differences in liquefaction characteristics between the fully saturated and the gassy sand. Both the fully saturated and gassy sand show the cyclic liquefaction feature because of the cumulative shear shrinkage in the early stage of the cyclic loading, and the alternation behavior between the shear dilatancy in the process of loading and the volume-contraction in the process of unloading in subsequent stages of cyclic loading.

The dynamic pore pressure properties of saturated sand are closely related to the volume change of soil skeleton, and they can reflect evolution properties of shear shrinkage, shear dilatancy and the volume-contraction in unloading process under the undrained condition, which has been reported in literatures (e.g. Wang 1997; Wang and Wang 2009). In order to explain the liquefaction mechanism of saturated sand under the undrained condition, Zhang (2000) believed that the

volumetric strain ε_v of saturated sand consisted of two basic components: ε_{vc} caused by the mean effective stress, and ε_{vd}

$$\varepsilon_v = \varepsilon_{vc} + \varepsilon_{vd} = 0 \tag{13}$$

caused by the shear stress. E_{vd} is further decomposed into a reversible and an irreversible component, namely $\varepsilon_{vd,re}$ and $\varepsilon_{vd,ir}$.

$$\varepsilon_{vd} = \varepsilon_{vd,ir} + \varepsilon_{vd,re} \tag{14}$$

$\varepsilon_{vd,ir}$ results from the extinction of macro void, reduction of average porosity, and crushing of particles. $E_{vd,re}$ refers to the reversal of shear expansion normally caused by the particle sliding and reorientation. E_{vc} results in a certain level of pore pressure accumulation; $\varepsilon_{vd,ir}$ results in the monotonic accumulation of dynamic pore pressure, and $\varepsilon_{vd,re}$ leads to the periodic fluctuation of dynamic pore pressure.

Different from the fully saturated sand, gas compressibility/expansibility, migration, dissolution/exsolution in gassy sand during cyclic loading have important influences on the volume change of sand skeleton. Because of the compressibility/expansibility of gas bubbles, under the same level of dynamic strain as saturated sand, ε_{vc} does not result in the same level of pore pressure accumulation. Because of the higher resistance of gas bubbles to pass through the sand voids (migration), under the same level of dynamic stress, $\varepsilon_{vd,ir}$ is smaller than saturated sand, but $\varepsilon_{vd,re}$ is larger. Those result in the slower accumulation of average dynamic pore pressure, much greater fluctuation of the amplitude of dynamic pore pressure and deeper groove shape of pore water for gassy sand. Meanwhile, gas exsolution promotes to cause $\varepsilon_{vd,re}$ and gas dissolution promotes to cause ε_{vc}. All of the effects exist in gassy sand during cyclic loading. In other words, gas existence slows down the residual liquefaction process of sand sediments, but it increases the risk of momentary liquefaction (Sumer et al. 2006).

Effects of initial gas content on liquefaction resistance

For gassy sand sediments, the free gas exists as isolated bubbles within the voids. The initial gas content of gassy sediments n_g' is defined as the ratio of the volume fraction of free gas bubbles n_g to the porosity of sediment soil n_0. That is, $n_g' = n_g/n_0$. Because n_g is equal to the volume of free gas divided by the total volume of sediments, there is a relationship between n_g' and the initial saturation S_r,

$$n_g' = 1 - S_r \tag{15}$$

Because S_r is easier to measure than n_g', the initial saturation S_r is used to describe the quantity of gas content n_g'. To study the initial gas content on the liquefaction resistance of gassy sand, a series of dynamic triaxial tests were performed on sand specimens with different initial saturations (S_r =100%, 97.6%, 94.1%, 92.3%).

Test results for liquefaction resistance of gassy sand under different initial saturations are shown in Table 2. Obviously, under each type of initial saturation, the number of cycles to

Table 2 Test results for liquefaction resistance of gassy sand under different gas contents

Specimen number	Initial gas content n_g' (%)	Initial saturation Sr (%)	Dynamic deviator stress σ_d (kPa)	Number of cycles to initial liquefaction N_f	CSR
101	0	100	10.0	9587	0.1
102			16.5	176	0.137
103			20.5	11	0.195
104			25.5	5	0.245
201	2.4	97.6	15.5	168	0.148
202			19.0	52	0.186
203			22.0	15	0.213
204			25.5	7	0.25
301	5.9	94.1	20.5	121	0.18
302			30.5	18	0.297
303			35.5	9	0.333
304			40.5	5	0.391
401	7.7	92.3	30.5	80	0.297
402			35.5	33	0.345
403			40.5	13	0.395

reach the initial liquefaction N_f decreases with the increase of applied dynamic deviator stress σ_d. The cyclic resistance often represents as the cyclic stress ratios (CSR), which is defined as the applied shear stress amplitude τ_d divided by initial vertical effective stress σ'_{v0} versus N_f. It can be seen that CSR of all specimens under different initial saturations decrease with the increase of N_f. Figure 13 shows the cyclic resistance curves of gassy sand under different initial saturations. From the figure, we can easily find the varying law of sand liquefaction resistance under different initial saturations (gas contents). The cyclic resistance of gassy sand is significantly affected by the initial gas content. For further analysis, the curves between CSR and the initial saturation within a certain number of cycles are shown in Fig. 14. For the twelfth, twentieth, and thirtieth stress cycles, it can be clearly found that the liquefaction resistance decreases with the increase of initial saturation.

Effects of initial gas content on evolutions of dynamic pore pressure

Liquefaction is the result of accumulation for pore water pressure under cyclic loading. The generation patterns of pore pressure under different initial saturations (or gas contents) are shown in Fig. 15. They are expressed as the dynamic pore pressure ratio u_d/σ'_{v0} (where u_d is the dynamic pore water pressure, σ'_{v0} is the initial vertical effective stress) versus the cycle ratio (it is defined as the loading cycle N normalized by N_f). The results show that evolutions of dynamic pore pressure are greatly affected by the initial gas content. In general, the higher the initial saturation degree, the larger the dynamic pore pressure ratio. It is found that a pore pressure generation function of saturated soil proposed by Seed also fits for the gassy sand (Seed et al. 1976). The equation of pore pressure evolution in undrained cyclic triaxial tests is described as follows:

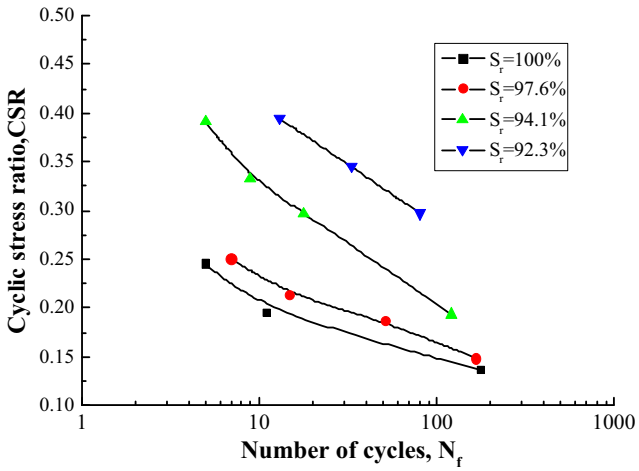

Fig. 13 CSR versus number of cycles to liquefaction for gassy sand

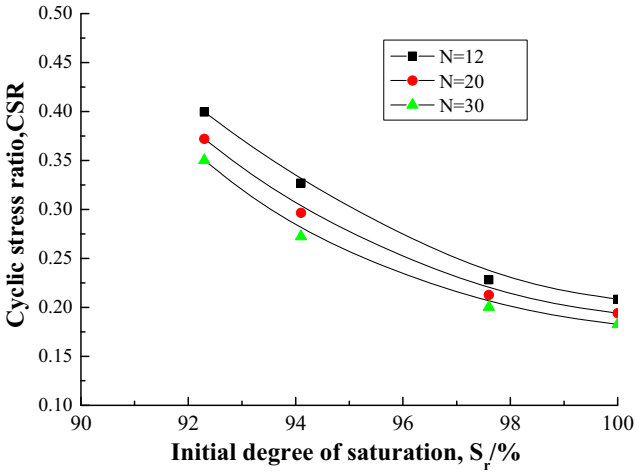

Fig. 14 CSR versus initial saturation degree at different cycles (N = 12, 20, 30)

$$\frac{u_d}{\sigma'_{v0}} = \frac{2}{\pi}\arcsin\left(\frac{N}{N_f}\right)^{\frac{1}{2\theta}} \tag{16}$$

where θ is an empirical constant, dependent on soil type and test conditions. For gassy sand, the θ values are 2.447, 1.947, 1.370, and 1.051 corresponding to different initial saturations 100%, 97.6%, 94.1%, and 92.3%, respectively. To understand better how the initial saturation degree (or gas content) affects dynamic pore pressure properties of gassy sand, the relationship between the change of θ and the initial saturation are shown in Fig. 16. The relation is approximately linear:

$$\theta = 17.9S_r - 15.5 \tag{17}$$

It can be seen that θ increases monotonously with the increasing initial saturation of gassy sand. The higher is the initial saturation of gassy sand, the larger is the value of θ

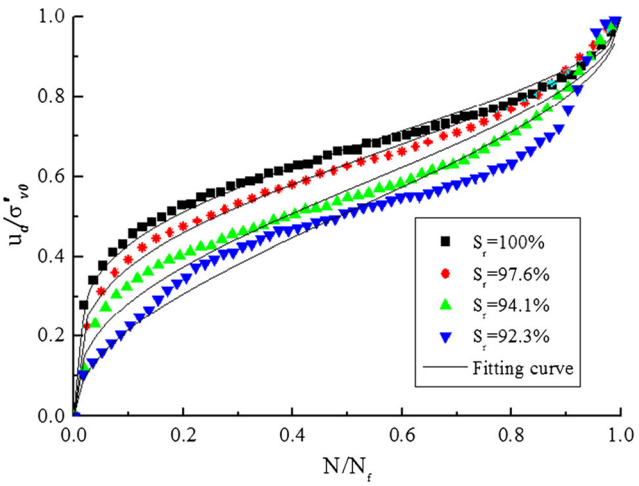

Fig. 15 Effects of initial saturation degree on relation between u_d/σ'_{v0} and N/N_f

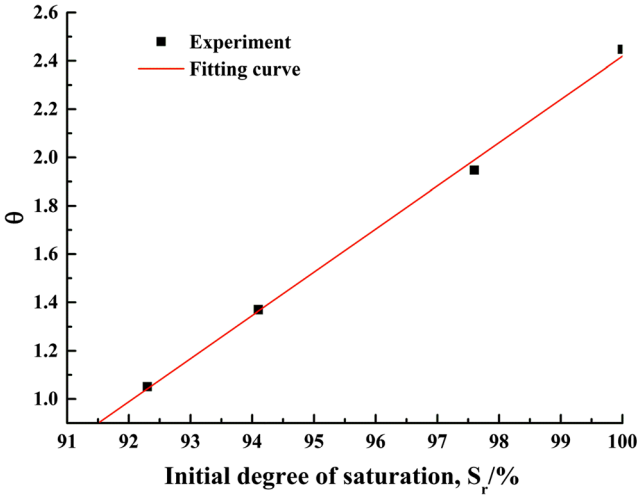

Fig. 16 The curve of parameter θ versus the initial saturation S_r

and the dynamic pore pressure ratio. By introducing a parameter of saturation S_r, Eq. (14) can be modified:

$$\frac{u_d}{\sigma'_{v0}} = \frac{2}{\pi}\arcsin\left(\frac{N}{N_f}\right)^{\frac{1}{2(aS_r-b)}} \tag{18}$$

where parameters a and b are empirical constants dependent on the soil type and test conditions. In this work, a = 17.9 and b = 15.5.

Conclusions

To investigate the effects of gas on the liquefaction characteristics of loose marine sand sediments, the triaxial gassy sand specimens with different initial gas contents (initial saturation ≥ 85%) but the same dry density were prepared in the lab by developing an effective methodology. A series of undrained dynamic triaxial tests by the GDS DYNNTTS were performed to study liquefaction characteristics of gassy sand with different initial saturations. The testing results and findings are summarized below:

(1) The occluded free gas bubbles have significant influences on sand liquefaction resistance, which monotonically increases with the decrease of initial gas content. However, once under a sufficiently large load (e.g. strong storm), the marine gassy sand sediments of shallow seafloor liquefy the same as the fully saturated sand.

(2) Because of the effects of gas compression/expansion, migration and dissolution/exsolution, the pore pressure buildup of gassy sand is slower than the saturated sand, and its dynamic pore pressure shows the obvious features of slower cumulative shear shrinkage of sand skeleton in process of loading and stronger volume-contraction in the process of unloading. Because of gas existence, which leads to different pore pressure buildup ratio for the fully saturated parts and gas-bearing parts of seafloor under cyclic loading, it tends to cause higher upward-directed gradient of pore water pressure so as to trigger momentary liquefaction of the marine shallow sediments.

(3) By introducing the parameter of saturation, a modified model was proposed to describe the evolution of dynamic pore pressure of marine gassy sand sediments. It is found that parameter θ is linear dependent on initial gas content (or initial saturation S_r).

Acknowledgments The research has been financially supported by the National Natural Science Foundation of China (Grant No. 51579237 and 51779017), the Foundation of State Key Laboratory for Geomechanics and Deep Underground Engineering (Grant No. SKLGDUEK 1110), the Natural Science Foundation of Zhejiang Province in China (Grant No. LY13E080009), and the Foundation of Changjiang River Scientific Research Institute of China (CKSF2017023/YT). The authors sincerely thank Prof. J. Z. Sun in Wuhan University of Technology and anonymous reviewers for their comments and suggestions to improve the manuscript.

References

Ahmad JM, Majid AA, Radu P (2007) Analysis of liquefaction susceptibility of nearly saturated sands. Int J Anal Met 31:691–714

Amaratunga A, Grozic JLH (2009) On the undrained unloading behaviour of gassy sands. Can Geotech J 46:1267–1276

Anderson AL, Abegg F, Hawkins JA, Duncan ME, Lyons AP (1998) Bubble populations and acoustic interaction with the gassy floor of Eckernforde Bay. Cont Shelf Res 18:1807–1838

Boudreau BP, Algar C, Johnson BD, Croudace I, Reed A, Furukawa Y, Dorgan KM, Jumars PA, Grader AS, Gardiner BS (2005) Bubble growth and rise in soft sediments. Geology 33:517–520

Christan HA, Woeller DJ, Robertson PK, Countney RC (1997) Site investigations to evaluate flow liquefaction slides at sand heads, Fraser River delta. Can Geotech J 34(3):384–397. https://doi.org/10.1139/cgj-34-3-384

Eseller-Bayat E (2009) Seismic response and prevention of liquefaction failure of sands partially saturated through introduction of gas bubbles. Dissertation, Northeastern University

Eseller-Bayat E, Yegian MK, Alshawabkeh A, Gokyer S (2013) Liquefaction response of partially saturated sands. II: Empirical model. J Geotech Geoenviron 139(6):872–879

Esrig MI, Kirby RC (1977) Implications of gas content for predicting stability of submarine slopes. Mar Geotechnol 2:81–100

Fleischer P, Orsi TH, Richardson MD, Anderson AL (2001) Distribution of free gas in marine sediments: a global overview. Geo-Mar Lett 21:103–122

Fredlund DG, Rahardjo H (1993) Soil mechanics for unsaturated soil. John Wiley & Sons, New York

Grozic JLH, Robertson PK, Morgenstern NR (1999) The behavior of loose gassy sand. Can Geotech J 36:482–492

Grozic JLH, Robertson PK, Morgenstern NR (2000) Cyclic liquefaction of loose gassy sand. Can Geotech J 37:843–856

Grozic JLH, Imam SMR, Robertson PK, Morgenstern NR (2005) Constitutive modeling of gassy sand behaviour. Can Geotech J 42(3):812–829

Gu XQ, Yang J, Huang MS (2013) Laboratory measurements of small strain properties of dry sands by bender element. Soils Found 53(5): 735–745

Ishihara K, Tsukamoto Y, Kamada K (2004) Undrained behavior of near-saturated sand in cyclic and monotonic loading. In: Proc. conf., cyclic behavior of soils and liquefaction phenomena, pp 27–39

Kokusho T (2000) Correlation of pore-pressure B-value with P-wave velocity and Poissen's ratio for imperfectly saturated sand or gravel. Soils Found 40(4):95–102

Ladd RS (1977) Specimen preparation and cyclic stability of sands. J Geotech Eng Div ASCE 103(6):535–547

Lee SH, Chough SK (2003) Distribution and origin of shallow gas in deep-sea sediments of the Ulleung Basin, East Sea. Geo-Mar Lett 22:204–209

Lings ML, Greening PD (2001) A novel bender/extender element for soil testing. Geotechnique 51(8):713–717

Mabrouk A, Rowe RK (2011) Effect of gassy sand lenses on a deep excavation in a clayed soil. Eng Geol 122:292–302

Nageswaran S (1983) Effect of gas bubbles on the sea bed behaviour. Dissertation, Oxford University

Oung JN, Lee CY, Kuo CL (2006) Geochemical study on hydrocarbon gases in seafloor sediments, southwestern offshore Taiwan - implications in the potential occurrence of gas hydrates. Terr Atmos Ocean Sci 17:921–931

Puzrin AM, Tront J, Schmid A, Hugues JB (2011) Engineered use of microbial gas production to decrease primary consolidation settlement in clayey soils. Geotechnique 61:785–794

Rad NS, Vianna AJD, Berre T (1994) Gas in soils. II: Effect of gas on undrained static and cyclic strength of sand. J Geotech Eng 120(4): 716–737

Rebata-Landa V, Santamarina JC (2012) Mechanical effects of biogenic nitrogen gas bubbles in soils. J Geotech Geoenviron 138:128–137

Seed HB, Martin PP, Lysmer J (1976) Pore-water pressure changes during soil liquefaction. J Geotech Eng Div ASCE 102(4):323–346

Sills GC, Gonzalez R (2001) Consolidation of naturally gassy soft soil. Geotechnique 51:629–639

Sills GC, Wheeler SJ (1992) The significance of gas for offshore operations. Cont Shelf Res 12(10):1239–1250

Sills GC, Wheeler SJ, Thomas SD, Gardner TN (1991) Behaviour of offshore soil containing gas bubbles. Geotechnique 41(2):227–241

Sobkowicz JC, Morgenstern NR (1984) The undrained equilibrium behaviour of gassy sediments. Can Geotech J 21(3):439–448

Sparks ADW (1963) Theoretical considerations of stress equations for partly saturated soils. In: Proceedings of the 3rd African conference on soil mechanics and foundation engineering, Salisbury, Rhodesia, 1, 215–218

Sultan N, De Gennaro V, Puech A (2012) Mechanical behaviour of gas-charged marine plastic sediments. Geotechnique 62:751–766

Sumer BM, Truelsen C, Fredsøe J (2006) Liquefaction around pipelines under waves. J Waterw Port Coast Ocean Eng 132(4):266–275

Tjelta TI, Svano G, Strout JM, Forsberg CF, Johansen H, Planke S (2007) Shallow gas and its multiple impact on North Sea production platform. Proceedings of the 6th int. offshore site investigation and geotechnics conference, London, 205–220

Van Kessel T, van Kesteren WGM (2002) Gas production and transport in artificial sludge depots. Waste Manag 22:19–28

Wang WS (1997) The dynamic strength and liquefaction characteristics of soil (in Chinese). Water Power Press, Beijing

Wang YL, Wang Y (2009) Experimental study on evolutionary characteristics of dynamic pore water pressure of saturated sands (in Chinese). J Tongji Univ (Nat Sci) 37(12):1603–1607

Wang Y, Kong LW, Wang YL, Wang M, Kejian C (2017) Deformation analysis of shallow gas-bearing ground from controlled gas release in Hangzhou Bay of China. Int J Geomech. https://doi.org/10.1061/(ASCE)GM.1943-5622.0001029

Wheeler SJ, Sills GC, Sham WM, Duffy SM, Boden DG (1991) The influence of shallow gas on the geotechnical properties of fine-grained sediments. J Soc Underw Technol 17(3):11–16

Wood FM, Yamamuro JA, Lade PV (2008) Effect of deposi-tional method on the undrained response of silty sand. Can Geotech J 45(11): 1525–1537

Yamamuro JA, Wood FM (2004) Effect of depositional method on the undrained behavior and microstructure of sand with silt. Soil Dyn Earthq Eng 24:751–760

Yong J (2002) Liquefaction resistance of sand in relation to p-wave velocity. Geotechnique 52(4):295–298

Yoshimichi T, Kenji I, Hiroshi N, Kunio K, Yongnan H (2002) Resistance of partly saturated sand to liquefaction with reference to longitudinal and shear wave velocities. Soils Found 42(6):93–104

Yoshimichi T, Shohei K, Matsumoto J, Shotaro H (2014) Cyclic resistance of two silty sands against soil liquefaction. Soils Found 54(6): 1094–1103

Zhang JM (2000) Reversible and irreversible dilatancy of sand (in Chinese). Chin J Geotech Eng 1(22):7–12